Pseudopotential calculations of electron and hole addition spectra of InAs, InP, and Si quantum dots

Alberto Franceschetti and Alex Zunger
National Renewable Energy Laboratory, Golden, Colorado 80401
(Received 5 November 1999)

The electron and hole addition energies, the quasiparticle gap, and the optical gap of InAs, InP, and Si quantum dots are calculated using microscopic pseudopotential wave functions. The effects of the dielectric mismatch between the quantum dot and the surrounding material are included using a realistic profile for the dielectric constant $\epsilon(\mathbf{r})$. We find that the addition energies and the quasiparticle gap depend strongly on the dielectric constant of the environment ϵ_{out}, while the optical gap is rather insensitive to ϵ_{out}. We compare our results with recent tunneling spectroscopy measurements for InAs nanocrystals, finding excellent agreement. Our calculations for the addition energies and the quasiparticle gap of InP and Si nanocrystals serve as predictions for future experiments.

I. INTRODUCTION: THE PHYSICAL INTERPRETATION OF ELECTRON AND HOLE CHARGING ENERGIES

Semiconductor quantum dots can be made with various dielectric coatings: Organic molecules,[1,2] other semiconductors (e.g., self-assembled dots,[3] core-shell nanocrystals,[4] lithographically etched dots,[5] strain-induced dots[6]), or glasses.[7] It has been realized[8,9] that the dielectric environment can profoundly affect the optical and transport properties of semiconductor quantum dots. This can be seen by considering a quantum dot of dielectric constant ϵ_{in} surrounded by a material of dielectric constant ϵ_{out}, subject to the three processes described in Fig. 1: (a) electron addition, (b) creation of an electron-hole pair, and (c) optical excitation.

(a) Electron addition. Figure 1(a) depicts the process of sequentially adding three electrons to an otherwise neutral quantum dot. The initial configuration of the system (of energy E_0) consists of the neutral dot in the ground state and a Fermi reservoir at the reference energy $\varepsilon_{\text{ref}} \equiv 0$. The energy of the quantum dot with one electron added to the conduction level e_1 is

$$E_1[e_1] = E_0 + \varepsilon_{e1}. \tag{1}$$

The electron quasiparticle energy $\varepsilon_{e1} = \varepsilon^0_{e1} + \Sigma^{\text{pol}}_{e1}$ can be separated into a single-particle contribution ε^0_{e1}, which describes *quantum confinement*, and a polarization contribution Σ^{pol}_{e1}, which describes *dielectric confinement*. The single-particle energy ε^0_{e1} is the energy of the added electron with respect to the reference energy ε_{ref} in the absence of dielectric mismatch. Σ^{pol}_{e1} is the self-energy of the added electron in the electrostatic field generated by its own image charge due to the dielectric constant discontinuity ($\epsilon_{\text{out}} \neq \epsilon_{\text{in}}$) at the surface of the dot.[9] The ''charging energy'' μ_1 required to load the first electron from the reservoir into the quantum dot is then

$$\mu_1 \equiv E_1[e_1] - E_0 = \varepsilon_{e1}. \tag{2}$$

The energy of the quantum dot with two electrons in the single-particle level e_1 is

$$E_2[e_1^2] = E_0 + 2\varepsilon_{e1} + J_{e1,e1}, \tag{3}$$

where $J_{e1,e1}$ is the total Coulomb interaction between the two electrons. $J_{e1,e1}$ includes a direct electron-electron contribution $J^{\text{dir}}_{e1,e1}$ (screened by the dielectric constant of the quantum dot), and a polarization contribution $J^{\text{pol}}_{e1,e1}$, which arises from the interaction of one electron with the image charge of the other electron across the dielectric discontinuity at the surface of the dot.[9] The charging energy μ_2 required to add the second electron to the quantum dot is then

$$\mu_2 \equiv E_2[e_1^2] - E_1[e_1^1] = \varepsilon_{e1} + J_{e1,e1}. \tag{4}$$

The energy of the quantum dot with two electrons in the single-particle level e_1 and one electron in the single-particle level e_2 is

$$E_3[e_1^2 e_2^1] = E_0 + 2\varepsilon_{e1} + \varepsilon_{e2} + J_{e1,e1} + 2J_{e1,e2} - K_{e1,e2}, \tag{5}$$

where $K_{e1,e2}$ is the exchange energy between the parallel spin electrons in the $e1$ and $e2$ single-particle levels. The charging energy μ_3 to add the third electron to the quantum dot is then

$$\mu_3 \equiv E_3[e_1^2 e_2^1] - E_2[e_1^2] = \varepsilon_{e2} + 2J_{e1,e2} - K_{e1,e2}. \tag{6}$$

The electron ''addition energies'' $\Delta^{(e)}_{N,N+1}$ are defined as the differences between the charging energies μ_N. For instance, the addition energy for the second electron is

$$\Delta^{(e)}_{1,2} \equiv \mu_2 - \mu_1 = J_{e1,e1}, \tag{7}$$

while the addition energy for the third electron is

$$\Delta^{(e)}_{2,3} \equiv \mu_3 - \mu_2 = (\varepsilon_{e2} - \varepsilon_{e1}) + (2J_{e1,e2} - J_{e1,e1}) - K_{e1,e2}. \tag{8}$$

Similar expressions can be written for the addition energies of the holes $\Delta^{(h)}_{N,N+1}$. For example, the addition energy of the second hole in the single-particle level h_1 is

$$\Delta^{(h)}_{1,2} \equiv \mu_{-1} - \mu_{-2} = J_{h1,h1}. \tag{9}$$

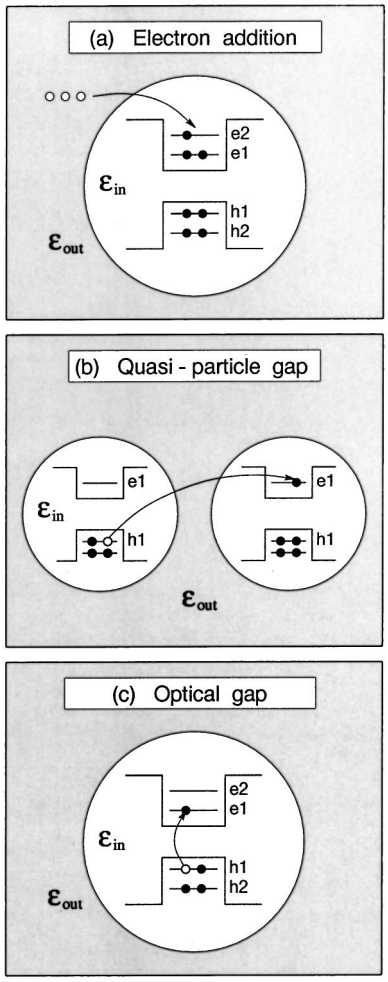

FIG. 1. Part (a) illustrates the process of loading three electrons into an otherwise neutral quantum dot. Part (b) shows the process of removing a single electron from a quantum dot and placing it into an identical dot at infinite distance. Part (c) describes the process of optically exciting an electron-hole pair in a neutral quantum dot.

The electron and hole charging energies μ_N and addition energies $\Delta_{N,N+1}$ can be measured by charging spectroscopies or tunneling spectroscopies.[5,10] Figure 2 shows a schematic diagram of the conductance/voltage spectrum of a quantum dot. The charging energies μ_N correspond to the peaks of the charging spectrum, while the addition energies $\Delta_{N,N+1}$ correspond to the spacings between the peaks. Since the polarization energies $\Sigma_i^{\rm pol}$ and $J_{i,j}^{\rm pol}$ depend strongly on the dielectric constant $\epsilon_{\rm out}$ of the surrounding material, the charging energies μ_N and the addition energies $\Delta_{N,N+1}$ depend on the dielectric environment.

(b) Creation of a noninteracting electron-hole pair. Figure 1(b) describes the process of removing an electron from the highest-energy valence-band level h_1 of a neutral quantum dot and placing it into the lowest-energy conduction-band level e_1 of an identical dot located at infinite distance from the first dot. The energy required by this process is the difference between the ionization potential and the electron affinity of the dot and corresponds to the energy of a noninteracting electron-hole pair (''quasiparticle gap''). The initial configuration, consisting of the two neutral dots in the ground state, has energy $2E_0$, while the final configuration

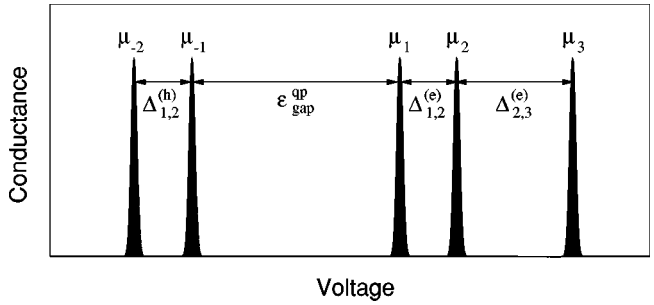

FIG. 2. Schematic diagram of the conductance/voltage spectrum of a semiconductor quantum dot. The charging energies μ_N correspond to the peaks in the conductance spectrum, while the addition energies $\Delta_{N,N+1}$ correspond to the spacings between the peaks.

has energy $E_1[e_1]+E_{-1}[h_1]$, where $E_{-1}[h_1]=E_0-\varepsilon_{h1}^0+\Sigma_{h1}^{\rm pol}$ is the energy of the quantum dot with a hole in the highest occupied orbital h_1. The quasiparticle gap is then

$$\varepsilon_{\rm gap}^{\rm qp}=E_1[e_1]+E_{-1}[h_1]-2\,E_0=\varepsilon_{\rm gap}^0+\Sigma_{e1}^{\rm pol}+\Sigma_{h1}^{\rm pol}, \tag{10}$$

where $\varepsilon_{\rm gap}^0\equiv\varepsilon_{e1}^0-\varepsilon_{h1}^0$ is the *single-particle* gap. For an infinitely large dot the polarization self-energies vanish, and the quasiparticle gap approaches the bulk single-particle gap: $\varepsilon_{\rm gap}^{\rm qp}\rightarrow\varepsilon_{\rm gap}^0$. The quasiparticle gap can be measured by tunneling spectroscopy experiments[10] as the difference $\varepsilon_{\rm gap}^{\rm qp}=\mu_1-\mu_{-1}$ between the energy required to load an electron into the quantum dot and the energy required to remove an electron from the quantum dot (Fig. 2). We see that the quasiparticle gap depends, via the polarization self-energies $\Sigma_{e1}^{\rm pol}$ and $\Sigma_{h1}^{\rm pol}$, on the dielectric environment.

(c) Creation of an interacting electron-hole pair via optical excitation. Figure 1(c) describes the process of optically exciting an electron from the highest occupied orbital h_1 to the lowest unoccupied orbital e_1 of a neutral quantum dot. The energy required by this process is the optical (or ''excitonic'') gap $\varepsilon_{\rm gap}^{\rm opt}$. The optical gap differs from the quasiparticle gap by the total electron-hole interaction:

$$\varepsilon_{\rm gap}^{\rm opt}=\varepsilon_{\rm gap}^{\rm qp}-J_{h1,e1}\,. \tag{11}$$

The electron-hole Coulomb energy $J_{h1,e1}$ consists of a direct Coulomb contribution $J_{h1,e1}^{\rm dir}$, which does not depend on $\epsilon_{\rm out}$, and a polarization contribution $J_{h1,e1}^{\rm pol}$, which depends strongly on $\epsilon_{\rm out}$. The polarization contribution $J_{h1,e1}^{\rm pol}$ tends to cancel the self-energy contribution $\Sigma_{h1}^{\rm pol}+\Sigma_{e1}^{\rm pol}$ to the quasiparticle gap [see Eq. (10)]. As a result, the optical gap depends weakly on the dielectric environment.

The purpose of the present work is to clarify the dependence of the three processes described in Fig. 1 on $\epsilon_{\rm out}$ and to provide quantitative predictions for the addition energies and the quasiparticle gap of InAs, InP, and Si quantum dots. We will discuss in detail the effects of dielectric mismatch on (a) the electron and hole addition energies $\Delta_{N,N+1}$, (b) the quasiparticle gap $\varepsilon_{\rm gap}^{\rm qp}$, and (c) the optical gap $\varepsilon_{\rm gap}^{\rm opt}$. We will also discuss how to extract the single-particle gap from measurements of $\varepsilon_{\rm gap}^{\rm qp}$ or $\varepsilon_{\rm gap}^{\rm opt}$. The practical significance of consider-

ing different dielectric media stems from the fact that, due to the long-range character of the Coulomb interaction and the exponential decay of the wave functions outside the quantum dot, dielectric confinement and quantum confinement can be physically separated. In fact, by changing the dielectric environment *far away* from the dot, while keeping the same barrier material next to the dot, one can control and tailor the electronic properties (such as $\Delta_{N,N+1}$ and $\varepsilon_{\rm gap}^{\rm qp}$) without affecting quantum confinement (i.e., the single-particle energies and wave functions).

II. PREVIOUS CALCULATIONS AND PRESENT OBJECTIVES

There are two basic approaches in the literature for calculations of addition energies. The ''standard model'' of addition spectra of quantum dots is the ''constant capacitance'' model,[11] which assumes that the addition energies $\Delta_{N,N+1}$ are constant and independent of the number of particle N: $\Delta_{N,N+1}=e^2/2C$, where C is the capacitance of the dot. This simple model has been quite successful at describing Coulomb blockade effects in large quantum dots, where the Coulomb energies (e.g., $J_{e1,e1}$) are much larger that the single-particle energy differences (e.g., $\varepsilon_{e2}-\varepsilon_{e1}$). However, this model fails to properly describe the addition spectrum of smaller quantum dots, where the single-particle energy spacings become comparable with the Coulomb energies.

A second class of models[12–21] treats the interplay between quantum confinement and Coulomb charging using the effective-mass approximation (EMA). However, the consequences of dielectric mismatch on the addition energies $\Delta_{N,N+1}$ were not discussed in these works. The effects of dielectric mismatch on the *optical gap* of quantum dots ($\varepsilon_{\rm gap}^{\rm opt}$) have been addressed by several authors[9,22–27] using the EMA. The most widely studied problem has been the dependence of the exciton energy on the dielectric constant of the surrounding material.[9,23–26] The charging energy required to add two electrons to a quantum dot[9,22,25] and the binding energy of an impurity in a quantum dot[25] have also been discussed in the EMA framework.

In the present work we advance a third approach to the calculation of addition energies, based on pseudopotential single-particle energies and wave functions. Recent pseudopotential calculations[28] have demonstrated the importance of using an atomistic description of the quantum dot electronic structure for calculating the electron-hole Coulomb and exchange energies. The pseudopotential approach provides an accurate description of the wave function decay outside the quantum dot and of the interband coupling due to quantum confinement, which are critical for a correct evaluation of the polarization and Coulomb energies in small nanocrystals.

III. METHOD OF CALCULATION

A. Single-configuration total energies and addition energies

We approximate the many-particle wave function Ψ_N of a system of N electrons in the conduction band of a quantum dot by a single Slater determinant constructed from the wave functions $\{\psi_n,\ n=1,\ldots,N\}$ of the N single-particle states occupied by N electrons. The corresponding total energy is

$$E_N=E_0+\sum_i\ (\varepsilon_i^0+\Sigma_i^{\rm pol})n_i+\sum_{i<j}\ (J_{i,j}-K_{i,j})n_in_j,\quad(12)$$

where ε_i^0 are the conduction-band single-particle energy levels, $\Sigma_i^{\rm pol}$ are the polarization self-energies, $J_{i,j}$ and $K_{i,j}$ are the electron-electron Coulomb and exchange energies, respectively, and n_i are the occupation numbers of the conduction-band single-particle states ($\Sigma_i n_i=N$). Equations (1), (3), and (5) are special cases of Eq. (12) for the configurations (e_1^1), (e_1^2), and $(e_1^2e_2^1)$, respectively. A similar equation holds for the total energy of a system of N holes in the valence band of the quantum dot:

$$E_{-N}=E_0+\sum_i\ (-\varepsilon_i^0+\Sigma_i^{\rm pol})p_i+\sum_{i<j}\ (J_{i,j}-K_{i,j})p_ip_j.\quad(13)$$

Here p_i,p_j are the hole occupation numbers ($\Sigma_i p_i=N$), and the single-particle energies are taken with a minus sign indicating that the corresponding electron is *removed* from the dot. The ground state Ψ_N^0 (of energy E_N^0) corresponds to the configuration that minimizes the total energy E_N. It need not coincide with the configuration in which the single-particle levels e_i are occupied in order of increasing energy.

The electron charging energy μ_N is defined as the energy required to add one electron to a quantum dot containing $N-1$ electrons in the conduction band:

$$\mu_N=E_N^0-E_{N-1}^0.\quad(14)$$

It is convenient to define the charging energy μ_{-N} of N holes as the energy required to add one electron (i.e., remove one hole) to a quantum dot containing N holes:

$$\mu_{-N}=E_{-N+1}^0-E_{-N}^0,\quad(15)$$

so that the charging energy of one hole is μ_{-1}.

The electron and hole addition energies are then

$$\Delta_{N,N+1}^{(e)}=\mu_{N+1}-\mu_N,\quad(16)$$

$$\Delta_{N,N+1}^{(h)}=\mu_{-N+1}-\mu_{-N}.\quad(17)$$

In Eqs. (12) and (13) we neglect (i) the coupling between different Slater determinants (i.e., configuration-interaction effects), and (ii) the response of the single-particle wave functions to the electrostatic field set up by the net charge (i.e., self-consistent effects). These assumptions are sufficiently accurate in small, three-dimensional quantum structures in the strong-confinement regime.[20,28,29] In Ref. 28 we compared the electron-hole Coulomb energies of quantum dots calculated using unperturbed single-particle wave functions with the results of a self-consistent Hartree calculation. We found that the Coulomb energies change by less than 5% when self-consistent effects are taken into account. Furthermore, in Ref. 29 we showed that the main effect of configuration interaction on the exciton energy levels is a nearly uniform down shift of a few meV.

B. Single-particle energies and wave functions

The single-particle energies ε_i^0 and wave functions $\psi_i(\mathbf{r},\sigma)$ are obtained here from the solution of the Schrödinger equation:

$$[-\nabla^2+V_{ps}(\mathbf{r})+\hat{V}_{nl}]\psi_i(\mathbf{r},\sigma)=\varepsilon_i^0\psi_i(\mathbf{r},\sigma). \tag{18}$$

Here $V_{ps}(\mathbf{r})$ is the total pseudopotential of the system (dot + surrounding material), and $\hat{V}_{nl}$ is a short-range operator that accounts for the nonlocal part of the potential as well as spin-orbit coupling. The local potential $V_{ps}(\mathbf{r})$ is calculated from the superposition of screened atomic pseudopotentials:

$$V_{ps}(\mathbf{r})=\sum_i v_\alpha(\mathbf{r}-\mathbf{R}_{i,\alpha}), \tag{19}$$

where $v_\alpha(\mathbf{r}-\mathbf{R}_{i,\alpha})$ is the atomic pseudopotential for an atom of type α located at the position $\mathbf{R}_{i,\alpha}$. The atomic pseudopotentials v_α are fitted to reproduce the measured bulk transition energies, deformation potentials, and effective masses, as well as the bulk single-particle wave functions calculated using density-functional theory in the local-density approximation.[30] The pseudopotentials used here are from Ref. 31 (InAs), Ref. 32 (InP), and Ref. 33 (Si).

Since only a few single-particle states in an energy window around the band gap are required in the calculation of the addition energies, we solve Eq. (18) using the folded spectrum method,[34,35] which allows one to calculate *selected* eigenstates of the Schrödinger equation with a computational cost that scales only linearly with the size of the system. In this approach, Eq. (18) is replaced by the folded-spectrum equation

$$[-\nabla^2+V_{ps}(\mathbf{r})+\hat{V}_{NL}-\varepsilon_{ref}]^2\psi_i(\mathbf{r},\sigma)=(\varepsilon_i^0-\varepsilon_{ref})^2\psi_i(\mathbf{r},\sigma), \tag{20}$$

where ε_{ref} is an *arbitrary* reference energy. The lowest energy eigenstate of Eq. (20) coincides with the solution of the Schrödinger equation [Eq. (18)] whose energy is closest to the reference energy ε_{ref}. Therefore, by choosing the reference energy in the band gap, the band edge states can be obtained by minimizing the functional $A[\psi]=\langle\psi|(\hat{H}-\varepsilon_{ref})^2|\psi\rangle$.

The solution of Eq. (20) is performed by expanding the wave functions $\psi_i(\mathbf{r},\sigma)$ in a plane-wave basis set. To this purpose, the total pseudopotential $V_{ps}(\mathbf{r})$ is defined in a periodically repeated supercell Ω containing the quantum dot and a portion of the surrounding material. The supercell Ω is sufficiently large to ensure that the solutions of Eq. (20) are converged within 1 meV. The single-particle wave functions can then be expanded as $\psi_i(\mathbf{r},\sigma)=\Sigma_{\mathbf{G}}c_i(\mathbf{G},\sigma)\exp(i\mathbf{G}\cdot\mathbf{r})$, where the sum runs over the reciprocal-lattice vectors $\mathbf{G}$ of the supercell Ω. The energy cutoff of the plane-wave expansion is the same used to fit the bulk electronic structure, to ensure that the band-structure consistently approaches the bulk limit for large quantum dots. The minimization of the functional $A[\psi]$ is carried out in the plane-wave basis set using a preconditioned conjugate-gradient algorithm. More details on the minimization procedure and the scaling with the system size can be found in Ref. 35.

C. Direct and polarization interparticle Coulomb energies

The interparticle Coulomb energies $\overline{J}_{i,j}$ (screened by the *macroscopic* dielectric constant) are given by

$$\overline{J}_{i,j}=e\sum_\sigma\int|\psi_i(\mathbf{r},\sigma)|^2\Phi_j(\mathbf{r})d\mathbf{r}, \tag{21}$$

where $\Phi_j(\mathbf{r})$ is the electrostatic potential energy generated by the charge distribution $\rho_j(\mathbf{r})=e\Sigma_\sigma|\psi_j(\mathbf{r},\sigma)|^2$ in a dielectrically inhomogeneous medium described by the position-dependent dielectric constant $\epsilon(\mathbf{r})$. The electrostatic potential $\Phi_j(\mathbf{r})$ satisfies the Poisson equation:

$$\nabla\cdot\epsilon(\mathbf{r})\nabla\Phi_j(\mathbf{r})=-4\pi\rho_j(\mathbf{r}). \tag{22}$$

The dielectric constant $\epsilon(\mathbf{r})$ changes smoothly from ϵ_{in} to ϵ_{out} at the interface between the dot and the barrier, with a transition region of the order of the interatomic bond-length. We use a cosinelike profile for $\epsilon(\mathbf{r})$ in the interfacial region between the dot and the barrier. The dielectric constant of the quantum dot ϵ_{in} depends on the dot radius R. We use a modified Penn model[29] to describe the size dependence of ϵ_{in}.

The Poisson equation [Eq. (22)] is solved on a real-space grid using a finite-difference discretization of the gradient operator. For a generic function $f(\mathbf{r})$, the gradient of f calculated at the grid point $\mathbf{r}_i\equiv(x_1,y_i,z_i)$ is

$$\begin{aligned}\nabla f(x_i,y_i,z_i)=&\frac{f(x_{i+1},y_i,z_i)-f(x_{i-1},y_i,z_i)}{x_{i+1}-x_{i-1}}\hat{\mathbf{x}}\\&+\frac{f(x_i,y_{i+1},z_i)-f(x_i,y_{i-1},z_i)}{y_{i+1}-y_{i-1}}\hat{\mathbf{y}}\\&+\frac{f(x_i,y_i,z_{i+1})-f(x_i,y_i,z_{i-1})}{z_{i+1}-z_{i-1}}\hat{\mathbf{z}}.\end{aligned} \tag{23}$$

The computational domain includes the quantum dot and a region of the surrounding material. The boundary conditions are obtained from a multipole expansion of the electrostatic potential.[28] After discretization of the gradient operator, the Poisson equation reduces to a linear system, which is solved using a conjugate-gradient minimization algorithm.

The total Coulomb energy $\overline{J}_{i,j}$ of Eq. (21) can be separated into two physically distinct contributions: (i) the direct Coulomb energy

$$\overline{J}_{i,j}^{\text{dir}}=\frac{e^2}{\varepsilon_{\text{in}}}\sum_{\sigma,\sigma'}\int\int\frac{|\psi_i(\mathbf{r},\sigma)|^2|\psi_j(\mathbf{r}',\sigma')|^2}{|\mathbf{r}-\mathbf{r}'|}d\mathbf{r}\,d\mathbf{r}', \tag{24}$$

which corresponds to the interaction between two electrons (or two holes) in the quantum dot as if the dielectric constant was uniform throughout the system, and identical to the macroscopic dielectric constant of the quantum dot ε_{in}; and (ii) the polarization energy

$$J_{i,j}^{\text{pol}}=\overline{J}_{i,j}-\overline{J}_{i,j}^{\text{dir}}, \tag{25}$$

which accounts for the effects of the dielectric mismatch at the interface between the quantum dot and the surrounding material and the ensuing surface polarization charge.

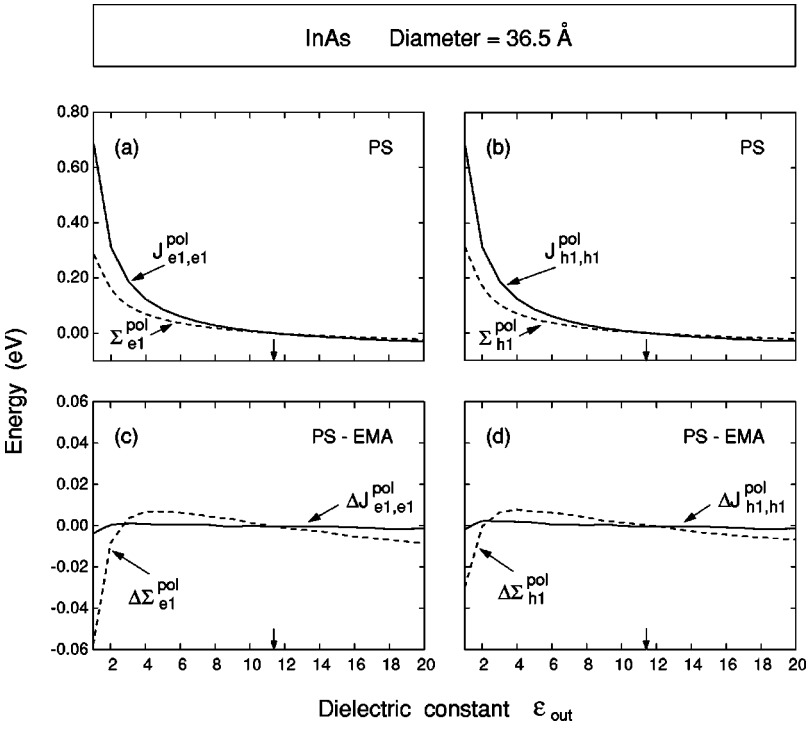

FIG. 3. The electron polarization energies $\Sigma_{e1}^{\rm pol}$ and $J_{e1,e1}^{\rm pol}$ [part (a)] and the hole polarization energies $\Sigma_{h1}^{\rm pol}$ and $J_{h1,h1}^{\rm pol}$ [part (b)] of an InAs quantum dot (diameter $D=36.5$ Å), calculated using pseudopotential wave functions, are shown as a function of the dielectric constant $\epsilon_{\rm out}$. Parts (c) and (d) shows the difference between the polarization energies calculated using pseudopotential (PS) and effective-mass (EMA) wave functions. Vertical arrows indicate the value $\epsilon_{\rm out}=\epsilon_{\rm in}$.

The interparticle Coulomb energies $\overline{J}_{i,j}$ obtained from the solution of Eqs. (21) and (22) are screened by the *macroscopic* dielectric constant of the system. The *microscopic* dielectric function $\epsilon(\mathbf{r},\mathbf{r}')$, however, tends to 1 when $\mathbf{r}'\to\mathbf{r}$. As a result, the short-range interparticle interaction is essentially unscreened. Recent pseudopotential calculations have shown that for wave functions localized in a quantum dot this effect can significantly enhance the electron-hole interaction. Therefore, we calculate the interparticle Coulomb energies $J_{i,j}$ as

$$J_{i,j}=J_{i,j}^{\rm dir}+J_{i,j}^{\rm pol}, \tag{26}$$

where $J_{i,j}^{\rm pol}$ is the polarization contribution obtained from Eq. (25) and $J_{i,j}^{\rm dir}$ is the direct Coulomb energy calculated using the microscopic dielectric function of the quantum dot:

$$J_{i,j}^{\rm dir}=e^2\sum_{\sigma,\sigma'}\int\int\frac{|\psi_i(\mathbf{r},\sigma)|^2|\psi_j(\mathbf{r}',\sigma')|^2}{\epsilon_{\rm in}(\mathbf{r},\mathbf{r}';R)|\mathbf{r}-\mathbf{r}'|}d\mathbf{r}\,d\mathbf{r}'. \tag{27}$$

The dielectric function $\epsilon_{\rm in}(\mathbf{r},\mathbf{r}';R)$ is decomposed into an electronic part $\epsilon_{\rm el}$ and an ionic part $\epsilon_{\rm ion}$, such that $1/\epsilon_{\rm in}=1/\epsilon_{\rm el}+1/\epsilon_{\rm ion}$. The electronic contribution $\epsilon_{\rm el}(\mathbf{r},\mathbf{r}';R)$ is approximated following the Thomas-Fermi model proposed by Resta:[36]

$$\frac{1}{\epsilon_{\rm el}(\mathbf{r},\mathbf{r}';R)}=\begin{cases}[\sinh q(\rho_\infty-|\mathbf{r}-\mathbf{r}'|)+q|\mathbf{r}-\mathbf{r}'|]/\epsilon_\infty^{\rm dot}(R)q\rho_\infty \\ \quad \text{if } |\mathbf{r}-\mathbf{r}'|\leqslant\rho_\infty \\ 1/\epsilon_\infty^{\rm dot}(R) \quad \text{if } |\mathbf{r}-\mathbf{r}'|\geqslant\rho_\infty,\end{cases} \tag{28}$$

where $q=2\pi^{-1/2}(3\pi^2 n_0)^{1/3}$ is the Thomas-Fermi wave vector corresponding to the quantum dot charge density n_0. The screening radius ρ_∞ is the solution of the equation $\sinh(q\rho_\infty)/(q\rho_\infty)=\epsilon_\infty^{\rm dot}(R)$, where $\epsilon_\infty^{\rm dot}(R)$ is the electronic contribution to the macroscopic dielectric constant of the quantum dot, which is obtained here using a modified Penn model.[29] As shown by Eq. (28), the electronic dielectric constant $\epsilon_{\rm el}(\mathbf{r},\mathbf{r}';R)$ approaches 1 when $|\mathbf{r}-\mathbf{r}'|\to 0$, and coincides with $\epsilon_\infty^{\rm dot}(R)$ when $|\mathbf{r}-\mathbf{r}'|\geqslant\rho_\infty$. Note that ρ_∞ is typically on the order of a few Å. The ionic contribution $\epsilon_{\rm ion}(\mathbf{r},\mathbf{r}';R)$ is approximated following the polaronic model of Haken.[37] For an electron-hole pair:

$$\frac{1}{\epsilon_{ion}(\mathbf{r},\mathbf{r}';R)}=\left[\frac{1}{\epsilon_0^{\rm dot}(R)}-\frac{1}{\epsilon_\infty^{\rm dot}(R)}\right]\times\left[1-\frac{\exp(-|\mathbf{r}-\mathbf{r}'|/\rho_h)+\exp(-|\mathbf{r}-\mathbf{r}'|/\rho_e)}{2}\right]. \tag{29}$$

Here $\rho_{h,e}=(\hbar/2m_{h,e}\omega_{LO})^{1/2}$, where $m_{h,e}$ denotes the hole (h) and electron (e) effective mass and ω_{LO} is the frequency of the bulk LO-phonon mode. The macroscopic dielectric constant $\epsilon_0^{\rm dot}(R)=\epsilon_\infty^{\rm dot}(R)+\Delta\epsilon_{\rm ion}$ includes the electronic contribution $\epsilon_\infty^{\rm dot}(R)$ and the ionic contribution $\Delta\epsilon_{\rm ion}$, which we assume to be size-independent.[29] As the radius of the quantum dot becomes small compared to ρ_h and ρ_e, the relative importance of ionic screening decreases.

The polarization energies $J_{e1,e1}^{\rm pol}$ and $J_{h1,h1}^{\rm pol}$ of a 36.5-Å-diameter InAs nanocrystals are shown in Figs. 3(a) and 3(b) as a function of the external dielectric constant $\epsilon_{\rm out}$. We see that $J_{h1,h1}^{\rm pol}$ and $J_{e1,e1}^{\rm pol}$ depend strongly on $\epsilon_{\rm out}$, and vanish when $\epsilon_{\rm out}=\epsilon_{\rm in}$. When $\epsilon_{\rm out}>\epsilon_{\rm in}$ the polarization energies become negative, thus acting to reduce the electron-electron (or hole-hole) interaction. The pseudopotential-

calculated polarization energies are compared in Figs. 3(c) and 3(d) with the results of an EMA calculation assuming (i) an infinite potential barrier at the surface of the quantum dot, and (ii) a purely *s*-like envelope function.[9] We see that the EMA calculation agrees well with the pseudopotential calculation, the difference being less than 5 meV across the entire range of values of $\epsilon_{\rm out}$. This suggests that the polarization energies $J^{\rm pol}_{i,j}$ are rather insensitive to the details of the electron and hole charge distributions.

D. Polarization self-energies

The polarization self-energies $\Sigma^{\rm pol}_i$ are given by

$$\Sigma^{\rm pol}_i = \frac{e}{2}\sum_\sigma \int \psi^*_i(\mathbf{r},\sigma) V_S(\mathbf{r}) \psi_i(\mathbf{r},\sigma) d\mathbf{r}, \tag{30}$$

where

$$V_S(\mathbf{r}) = \lim_{\mathbf{r}'\to\mathbf{r}} [G(\mathbf{r},\mathbf{r}') - G_{\rm bulk}(\mathbf{r},\mathbf{r}')]. \tag{31}$$

Here $G(\mathbf{r},\mathbf{r}')$ is the Green's function associated with the Poisson equation [Eq. (22)], and $G_{\rm bulk}(\mathbf{r},\mathbf{r}')$ is the bulk Green's function. We use the analytical expression[23] of $V_S(\mathbf{r})$ for a spherical quantum dot of dielectric constant $\epsilon_{\rm in}$ embedded in a medium of dielectric constant $\epsilon_{\rm out}$:

$$V_S(r) = \frac{e}{2R}\sum_{l=0}^{\infty} \frac{\epsilon_{\rm in}-\epsilon_{\rm out}}{\epsilon_{\rm out}+l(\epsilon_{\rm in}+\epsilon_{\rm out})} \times \begin{cases} \dfrac{(l+1)(r/R)^{2l}}{\epsilon_{\rm in}} & \text{if } r<R, \\ \dfrac{-l\,(r/R)^{-2(l+1)}}{\epsilon_{\rm out}} & \text{if } r>R. \end{cases} \tag{32}$$

Note that $V_S(r)$ vanishes when $\epsilon_{\rm out}=\epsilon_{\rm in}$, and that if $\epsilon_{\rm out}<\epsilon_{\rm in}$ the polarization potential is positive for $r<R$ and negative for $r>R$. The singularity of $V_S(r)$ at the surface of the dot ($r\to R$) is removed by applying a smoothing function $1-e^{-(r-R)^2/\lambda^2}$, where λ is a broadening factor of the order of the interatomic bond length.

Figures 3(a) and 3(b) show the electron and hole polarization self-energies $\Sigma^{\rm pol}_{e1}$ and $\Sigma^{\rm pol}_{h1}$ of a 36.5-Å-diameter InAs nanocrystal as a function of the external dielectric constant $\epsilon_{\rm out}$. The pseudopotential result is compared in Figs. 3(c) and 3(d) with an EMA calculation that assumes an infinite potential barrier at the surface of the nanocrystal.[38] We see that for $\epsilon_{\rm out}\ll\epsilon_{\rm in}$ the EMA polarization self-energies are significantly underestimated because the part of the wave function localized outside the dot (which is absent in the infinite-barrier EMA calculation) experiences a negative polarization potential.

The electron and hole self-energies of small Si nanocrystals have been recently calculated from first principles using the GW approximation.[39] It was found that the GW electron and hole self-energies are in excellent agreement with the results obtained from the classical electrostatic model of Eq. (32).

IV. RESULTS

We consider here InAs, InP, and Si spherical nanocrystals of diameter D ranging from $\sim$27 to $\sim$42 Å. All the dots have the T_d point-group symmetry. The surface dangling bonds are passivated using either ligandlike potentials [in the case of InP (Ref. 32) and Si (Ref, 33) nanocrystals] or a large-gap barrier material (in the case of InAs nanocrystals[31]). The passivating potential effectively removes the dangling-bond states from the band gap. The electronic structure is rather insensitive to the details of the passivating potential, since the near-band-edge states are localized in the interior of the nanocrystal. We assume that the atoms in the dot are located at their ideal bulk positions. Recent *ab initio* total-energy calculations[40] for small ($\sim$120 atoms) hydrogen-passivated silicon nanocrystals have shown that the Si-Si interatomic bond length changes by less than 1% compared to the bulk equilibrium bond length.

A. Single-particle energy levels and symmetries

The near-band-edge single-particle energy levels are summarized in Table I, together with the symmetry of the corresponding wave functions. Figure 4 shows schematically the energy level diagrams of InAs, InP, and Si dots. Each energy level in Table I and Fig. 4 is doubly degenerate because of time-reversal symmetry and can be occupied by two particles (electrons or holes). We note the following. (i) In the case of InAs and InP dots the two degenerate single-particle levels at the top of the valence band (h_1 and h_2) originate from the bulk Γ_{8v} states and have an *s*-like envelope function. The next two degenerate hole levels (h_3 and h_4) are also Γ_{8v} derived, but have *p*-like envelope functions. The electron level at the bottom of the conduction band (e_1) originates from the bulk Γ_{6c} state and has an *s*-like envelope function. The next three single-particle electron levels (e_2, e_3, and e_4) have a different origin in InAs and InP quantum dots. In InAs dots e_2, e_3, and e_4 derive from the bulk Γ_{6c} state and have a *p*-like envelope function[31] (e_2 is split from e_3 and e_4 because of spin-orbit splitting, as well as numerical approximations in the nonlocal pseudopotential), while in InP dots they originate from the L_{6c} bulk states and have an *s*-like envelope function.[32] (ii) In the case of Si dots (where spin-orbit coupling is small, and thus is not included in the calculations) the three t_2 degenerate levels at the top of the valence band originate from the bulk Γ_{15v} states and have an *s*-like envelope function, while the six levels at the bottom of the conduction band originate from the bulk conduction-band minima located near the X points of the Brillouin zone and have an *s*-like envelope function.[41] These electron states can be classified according to their point-group symmetry as t_2, a_1, or e.

B. Electron and hole addition energies

The electron and hole addition energies $\Delta_{N,N+1}$ are calculated using Eqs. (16) and (17). In calculating them we make the following approximations: (i) The ground-state configuration calculated for $\epsilon_{\rm out}=\epsilon_{\rm in}$ is also used for other values of ϵ_{out}. Since the Coulomb energies $J_{i,j}$ depend weakly on $\epsilon_{\rm out}$ in a relatively wide range of values around $\epsilon_{\rm out}=\epsilon_{\rm in}$ (see Fig. 3), the ground-state configuration should

TABLE I. Near-band-edge single particle states of passivated, spherical nanocrystals. The energies are measured with respect to the highest occupied state ($h1$). The point-group symmetry of the single-particle wave functions of Si nanocrystals is indicated in parentheses. InAs results are from Ref. 31, InP from Ref. 32, and Si from Ref. 33.

Valence level	Energy (eV)	Symmetry	Conduction level	Energy (eV)	Symmetry
		InAs	Diameter = 30.3 Å		
h1, h2	0.000	Γ_{8v}, *s*-like	$e1$	1.706	Γ_{6c}, *s*-like
h3, h4	−0.038	Γ_{8v}, *p*-like	e2	2.109	Γ_{6c}, *p*-like
			$e3$, $e4$	2.110	Γ_{6c}, *p*-like
		InAs	Diameter = 36.5 Å		
h1, h2	0.000	Γ_{8v}, *s*-like	$e1$	1.498	Γ_{6c}, *s*-like
h3, h4	−0.023	Γ_{8v}, *p*-like	$e2$	1.890	Γ_{6c}, *p*-like
			$e3$, $e4$	1.902	Γ_{6c}, *p*-like
		InAs	Diameter = 42.2 Å		
h1, h2	0.000	Γ_{8v}, *s*-like	$e1$	1.310	Γ_{6c}, *s*-like
h3, h4	−0.014	Γ_{8v}, *p*-like	$e2$	1.670	Γ_{6c}, *p*-like
			$e3$, $e4$	1.671	Γ_{6c}, *p*-like
		InP	Diameter = 28.0 Å		
h1, h2	0.000	Γ_{8v}, *s*-like	$e1$	2.404	Γ_{6c}, *s*-like
h3, h4	−0.089	Γ_{8v}, *p*-like	$e2$	2.667	L_{6c}, *s*-like
			$e3$, $e4$	2.725	L_{6c}, *s*-like
		InP	Diameter = 34.8 Å		
h1, h2	0.000	Γ_{8v}, *s*-like	$e1$	2.124	Γ_{6c}, *s*-like
h3, h4	−0.053	Γ_{8v}, *p*-like	$e2$, $e3$	2.432	L_{6c}, *s*-like
			$e4$	2.442	L_{6c}, *s*-like
		Si	Diameter = 27.0 Å		
h1, h2, h3	0.000	Γ_{15v}, *s*-like (t_2)	$e1$, $e2$	2.117	X_{1c}, *s*-like (e)
			$e3$	2.133	X_{1c}, *s*-like (a_1)
			$e4$, $e5$, $e6$	2.137	X_{1c}, *s*-like (t_2)
		Si	Diameter = 34.6 Å		
h1, h2, h3	0.000	Γ_{15v}, *s*-like (t_2)	$e1$, $e2$, $e3$	1.814	X_{1c}, *s*-like (t_2)
			$e4$	1.819	X_{1c}, *s*-like (a_1)
			$e5$, $e6$	1.822	X_{1c}, *s*-like (e)

be unchanged in this range. For smaller values of ϵ_{out} (i.e., $\epsilon_{\text{out}} \sim 1-4$) the ground-state configuration may be different from the ground-state configuration at $\epsilon_{\text{out}} = \epsilon_{\text{in}}$. However, the difference in the addition energies will be of the order of a few meV, i.e., only a few percent of the addition energies themselves. (ii) We neglect the contribution of the exchange energies $K_{i,j}$, which are about an order of magnitude smaller than the Coulomb energies $J_{i,j}$.

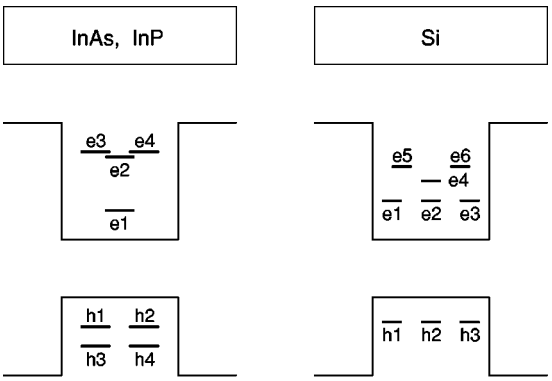

FIG. 4. Schematic diagram of the near-band-edge single-particle energy levels of InAs, InP, and Si spherical quantum dots.

The addition energies $\Delta_{N,N+1}$ of a few representative dots are shown in Fig. 5 for a few values of the external dielectric constant ϵ_{out}. The following features can be noted: (i) The electron and hole addition energies depend strongly on ϵ_{out}. This is due to the contribution of the polarization energies $J_{i,j}^{\text{pol}}$ to the addition energies $\Delta_{N,N+1}$ [see, for example, Eqs. (7) and (8)]. (ii) The electron addition energies of InAs and InP quantum dots show a pronounced peak for $N=2$ (corresponding to $\Delta_{2,3}^{(e)}$). This peak is due to the filling of the *s*-like shell: adding a third electron to a quantum dot that already contains two electrons in the *s*-like shell requires occupying a level of the *p*-like shell, which is about 0.3–0.4 eV higher in energy (see Table I). The effects of single-particle gaps on the addition spectrum are neglected in constant capacitance models. (iii) A less pronounced peak appears in the electron addition spectrum of InAs dots for $N=8$. This peak corresponds to the filling of the *p*-like shell. (iv) Since the six lowest-energy conduction levels of Si dots originate from the bulk X_{1c} valley and are very close in energy (see Table I), the electron addition spectrum of Si dots appears featureless up to $N=11$. (v) The hole addition energies are relatively constant as a function of N up to $N=7$. This is a consequence of the fact that the hole single-particle energy levels are closely spaced, so the addition energies are almost entirely determined by the hole-hole Coulomb energies.

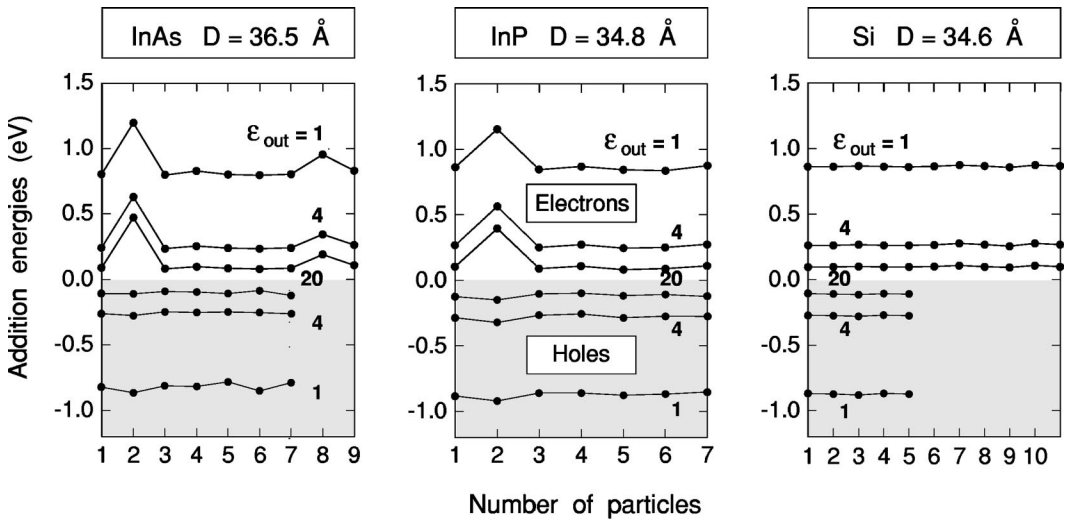

FIG. 5. Electron and hole addition energies of InAs, InP, and Si nanocrystals for a few values of the dielectric constant ϵ_{out} ($\epsilon_{\text{out}}=1, 4, 20$). For clarity purposes the hole addition energies are taken with a minus sign.

The addition energies of InAs nanocrystals have been recently measured by Banin *et al.*[10] using scanning tunneling spectroscopy. In these experiments the dielectric constant of the environment (ϵ_{out}) is an unknown quantity, as it corresponds to an average over the gold contact, the hexane dithiol linking molecules, and the organic passivants.[10] To compare our calculations with the experimental results we first fit our calculated value of the addition energy $\Delta_{1,2}^{(e)}$ for the $D=30.3$ Å InAs dot with the experimental value $\Delta_{1,2}^{(e)}=0.22$ eV for the nearest size dot ($D=34$ Å), finding that $\epsilon_{\text{out}}=6$ gives a good fit. We then use this value of ϵ_{out} to calculate the addition energies and the quasiparticle gap of InAs nanocrystals as a function of size. The calculated electron and hole addition energies $\Delta_{N,N+1}$ are compared in Fig. 6(a) with the experimental results of Banin *et al.*[10] We see that we have a very good agreement for $\Delta_{1,2}^{(h)}$ and $\Delta_{1,2}^{(e)}$ using a single value of ϵ_{out}. The calculated addition energy for the third electron, $\Delta_{2,3}^{(e)}$, is somewhat smaller than the experimental value. However, the nanocrystal size measured by scanning-tunneling microscopy (STM) tends to be overestimated,[10] and the actual size of the nanocrystals may be smaller. This would bring our results into even closer agreement with experiment.

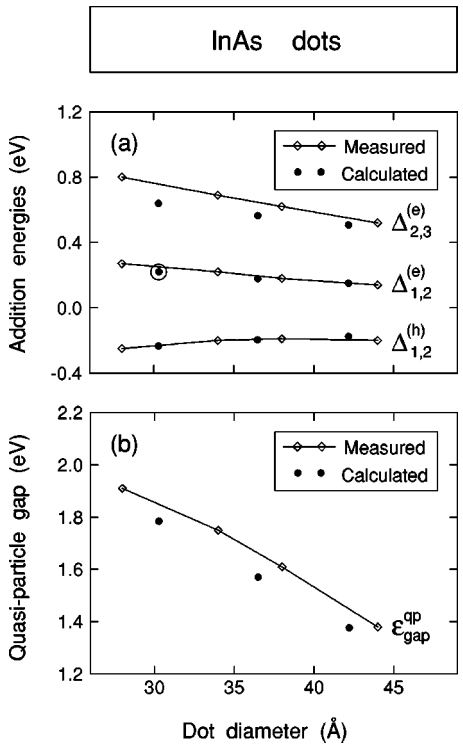

FIG. 6. The electron and hole addition energies [part (a)] and the quasiparticle gap [part (b)] of InAs nanocrystals, calculated for $\epsilon_{\text{out}}=6$, are compared with the experimental data of Banin *et al.* (Ref. 10) as a function of size. The circle in part (a) denotes the addition energy used to fit the value of ϵ_{out}. For clarity purposes, the hole addition energy $\Delta_{1,2}^{(h)}$ is taken with a minus sign.

C. Quasiparticle gap and optical gap

The quasiparticle gap [defined by Eq. (10)] represents the energy of a *noninteracting* electron-hole pair in a quantum dot, while the optical gap [defined by Eq. (11)] is the energy of an *interacting* electron-hole pair in the quantum dot.

The quasiparticle gap of Si nanocrystals in vacuum ($\epsilon_{\text{out}}=1$) was calculated by Öğüt, Chelikowsky, and Louie[42] using density-functional theory in the local-density approximation (LDA). They calculated the ground-state total energies E_1^{LDA} and E_{-1}^{LDA} of the charged nanocrystals as well as the ground-state energy E_0^{LDA} of the neutral dot, and obtained the quasi-particle gap as $\varepsilon_{\text{gap}}^{\text{qp, LDA}}=E_1^{LDA}+E_{-1}^{LDA}-2E_0^{LDA}$. For a $\sim$27-Å-diameter Si nanocrystal the LDA-calculated quasiparticle gap was $\varepsilon_{\text{gap}}^{\text{qp, LDA}}\sim 2.5$ eV. However, it is well known[43] that in the bulk limit the expression $E_1^{LDA}+E_{-1}^{LDA}-2E_0^{LDA}$ yields the LDA single-particle gap, which in the case of Si is about 0.68 eV lower than the bulk quasiparticle gap.[42] Therefore, the LDA-calculated quasi-particle gap of Si nanocrystals must also be underestimated.[43] Interestingly, if we estimate the LDA gap error in Si nanocrystals using the *bulk* LDA gap error of 0.68 Å, the quasiparticle gap be-

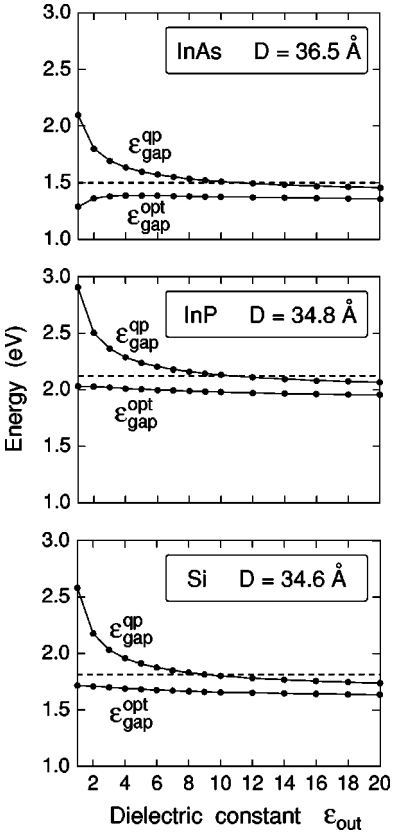

FIG. 7. Quasiparticle gap and optical gap of InAs, InP, and Si nanocrystals as a function of the dielectric constant ϵ_{out}. The dashed lines denote the single-particle gap $\varepsilon_{\text{gap}}^{0}$, which does not depend on ϵ_{out}.

comes $2.5+0.68\sim 3.2$ eV, which is in good agreement with our calculated value of 3.1 eV.

The quasiparticle gap of InAs nanocrystals was measured by Banin *et al.* using scanning-tunneling spectroscopy techniques.[10] Figure 6(b) compares the calculated quasiparticle gap (using $\epsilon_{\text{out}}=6$) with the experimental results of Banin *et al.*[10] As we can see the agreement is good, particularly if we take into account that the STM-measured size is overestimated.

Figure 7 shows the quasi-particle gap and the optical gap of a few representative nanocrystals as a function of the dielectric constant ϵ_{out}. Also shown is the single-particle gap $\varepsilon_{\text{gap}}^{0}=\varepsilon_{e1}^{0}-\varepsilon_{h1}^{0}$, which is independent of ϵ_{out}. We can see that the quasiparticle gap depends strongly on ϵ_{out}, and decreases by almost 1 eV when ϵ_{out} changes from 1 to 20. This is a consequence of the fact that the polarization self-energies Σ_{h1}^{pol} and Σ_{e1}^{pol}, which enter the quasiparticle gap via Eq. (10), depend strongly on ϵ_{out} (see Fig. 3). On the other hand, the dependence of the optical gap on ϵ_{out} is rather weak, as we can see from Fig. 7. This can be understood by rewriting the optical gap of Eq. (11), with the help of Eq. (10), as

$$\begin{aligned}\varepsilon_{\text{gap}}^{\text{opt}}&=\varepsilon_{\text{gap}}^{\text{qp}}-(J_{h1,e1}^{\text{dir}}+J_{h1,e1}^{\text{pol}})\\&=\varepsilon_{\text{gap}}^{0}-J_{h1,e1}^{\text{dir}}+(\Sigma_{e1}^{\text{pol}}+\Sigma_{h1}^{\text{pol}}-J_{h1,e1}^{\text{pol}}).\end{aligned}\tag{33}$$

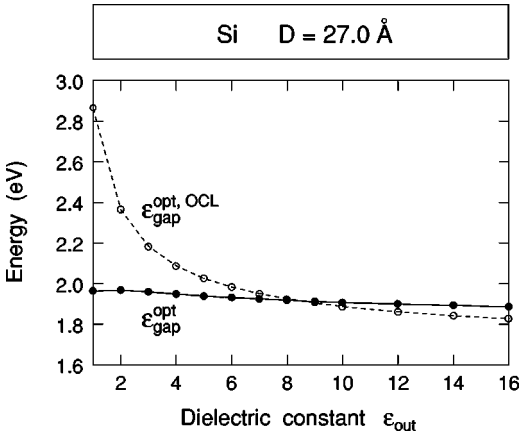

FIG. 8. The optical gap $\varepsilon_{\text{gap}}^{\text{opt}}$ of a 27.0-Å-diameter Si nanocrystal (solid line and filled circles) is compared with $\varepsilon_{\text{gap}}^{\text{opt, OCL}}$ calculated using Eq. (35) (dashed line and empty circles).

Since $\Sigma_{h1}^{\text{pol}}+\Sigma_{e1}^{\text{pol}}\simeq J_{h1,e1}^{\text{pol}}$ (see Fig. 3), the last term in parenthesis in Eq. (33) is small, and the optical gap can be approximately written as

$$\varepsilon_{\text{gap}}^{\text{opt}}\simeq\varepsilon_{\text{gap}}^{0}-J_{h1,e1}^{\text{dir}},\tag{34}$$

which does not depend on ϵ_{out}. This successful approximation has indeed been used in the literature for a long time.[9] Theorists correct their calculated single-particle gaps by subtracting the electron-hole Coulomb energy $J_{h1,e1}^{\text{dir}}$ to compare with experiment.[9]

A different form for $\varepsilon_{\text{gap}}^{\text{opt}}$ was suggested by Öğüt, Chelikowsky, and Louie.[42] They proposed to calculate the optical gap as

$$\varepsilon_{\text{gap}}^{\text{opt,OCL}}=\varepsilon_{\text{gap}}^{\text{qp}}-J_{h1,e1}^{\text{dir}}.\tag{35}$$

As shown by Eq. (33) this equation omits the polarization contribution $J_{h1,e1}^{\text{pol}}$, which is an integral part of the electron-hole interaction. As a result, the optical gap of Si nanocrystals in vacuum calculated by Öğüt *et al.*[42] is *overestimated*[44] compared to conventional calculations based on Eq. (33) or (34). This is shown in Fig. 8, where the optical gap $\varepsilon_{\text{gap}}^{\text{opt}}$ of Eq. (33) is compared with $\varepsilon_{\text{gap}}^{\text{opt, OCL}}$ calculated using Eq. (35). We see that for small values of ϵ_{out} Eq. (35) significantly overestimates the optical gap. The difference is as large as ~ 1 eV for $\epsilon_{\text{out}}=1$.

While $\varepsilon_{\text{gap}}^{\text{qp}}$ and $\varepsilon_{\text{gap}}^{\text{opt}}$ are measurable quantities, the single-particle gap $\varepsilon_{\text{gap}}^{0}$ is not, nor can it be derived from the knowledge of $\varepsilon_{\text{gap}}^{\text{qp}}$ and $\varepsilon_{\text{gap}}^{\text{opt}}$ without theoretical intervention. Using Eq. (34) the single-particle gap $\varepsilon_{\text{gap}}^{0}$ can be extracted from the optical gap $\varepsilon_{\text{gap}}^{\text{opt}}$ by adding back the direct Coulomb energy $J_{h1,e1}^{\text{dir}}$. Banin *et al.*[10] attempted to extract the single-particle gap from tunneling spectroscopy measurements by subtracting from the measured quasiparticle gap $\varepsilon_{\text{gap}}^{\text{qp}}=\mu_1-\mu_{-1}$ [Eq. (10)] the measured electron addition energy $\Delta_{1,2}^{(e)}=\mu_2-\mu_1$ [Eq. (7)]. However, as shown by Eq. (10), this procedure produces

$$\varepsilon_{\rm gap}^{\rm qp}-\Delta_{1,2}^{(e)}=\varepsilon_{\rm gap}^{0}+(\Sigma_{h1}^{\rm pol}+\Sigma_{e1}^{\rm pol}-J_{e1,e1})\neq\varepsilon_{\rm gap}^{0}. \quad (36)$$

The error is $(\Sigma_{h1}^{\rm pol}+\Sigma_{e1}^{\rm pol}-J_{e1,e1}^{\rm pol})-J_{e1,e1}^{\rm dir}\sim -J_{e1,e1}^{\rm dir}$. Thus, $\varepsilon_{\rm gap}^{\rm qp}-\Delta_{1,2}^{(e)}$ is *smaller* than $\varepsilon_{\rm gap}^{0}$ by an amount approximately equal to $J_{e1,e1}^{\rm dir}$.

V. SUMMARY

In conclusion, we predict the effects of the dielectric environment on the electron and hole addition energies of semiconductor quantum dots. Atomistic pseudopotential wave functions are used as input for the many-body expansion of the total energy of the charged dots. We find that the the addition energies and the quasiparticle gap depend sensitively on the dielectric constant $\epsilon_{\rm out}$ of the surrounding material via the self-energies $\Sigma_i^{\rm pol}$ and the polarization energies $J_{i,j}^{\rm pol}$. We compare the calculated addition energies of InAs nanocrystals with recent spectroscopic results,[10] finding excellent agreement for $\epsilon_{\rm out}=6$. Our calculations for Si and InP nanocrystals provide predictions for future single-electron charging experiments.

ACKNOWLEDGMENTS

The authors acknowledge useful discussions with F. Reboredo and A. Williamson. This work was supported by the U.S. DOE, OER-SC, Division of Materials Science, under Grant No. DE-AC36-98-GO10337.

[1] C.B. Murray, D.J. Norris, and M.G. Bawendi, J. Am. Chem. Soc. **115**, 8706 (1993).
[2] A.A. Guzelian, U. Banin, A.V. Kadavanich, X. Peng, and A.P. Alivisatos, Appl. Phys. Lett. **69**, 1432 (1996).
[3] D. Leonard, M. Krishnamurthy, C.M. Reaves, S.P. Denbaars, and P.M. Petroff, Appl. Phys. Lett. **63**, 3203 (1993).
[4] A.P. Alivisatos, Science **271**, 933 (1996).
[5] S. Tarucha, D.G. Austing, T. Honda, R.J. van der Hage, and L.P. Kouwenhoven, Phys. Rev. Lett. **77**, 3613 (1996).
[6] M. Sopanen, H. Lipsanen, and J. Ahopelto, Appl. Phys. Lett. **66**, 2364 (1995).
[7] A. Ekimov, J. Lumin. **70**, 1 (1996).
[8] L.V. Keldysh, Pis'ma Zh. Eksp. Teor. Fiz.**29**, 716 (1979) [JETP Lett. **29**, 658 (1979)].
[9] L.E. Brus, J. Chem. Phys. **79**, 5566 (1983); *ibid.* **80**, 4403 (1984).
[10] U. Banin, Y. Cao, D. Katz, and O. Millo, Nature (London) **400**, 542 (1999).
[11] C.W.J. Beenakker and H. von Houten, in *Single Charge Tunnelling*, edited by H. Grabert, J.M. Martinis, and M.H. Devoret (Plenum, New York, 1991).
[12] P.A. Maksym and T. Chakraborty, Phys. Rev. Lett. **65**, 108 (1990).
[13] P.L. McEuen, E.B. Foxman, U. Meirav, M.A. Kastner, Y. Meir, N.S. Wingreen, and S.J. Wind, Phys. Rev. Lett. **66**, 1926 (1991); P.L. McEuen, E.B. Foxman, J. Kinaret, U. Meirav, M.A. Kastner, N.S. Wingreen, and S.J. Wind, Phys. Rev. B **45**, 11 419 (1992).
[14] P. Hawrylak, Phys. Rev. Lett. **71**, 3347 (1993).
[15] J.J. Palacios, L. Martin-Moreno, G. Chiappe, E. Louis, and C. Tejedor, Phys. Rev. B **50**, 5760 (1994).
[16] A. Wojs and P. Hawrylak, Phys. Rev. B **53**, 10 841 (1996).
[17] L.R.C. Fonseca, J.L. Jimenez, J.P. Leburton, and R.M. Martin, Phys. Rev. B **57**, 4017 (1998).
[18] M. Rontani, F. Rossi, F. Manghi, and E. Molinari, Appl. Phys. Lett. **72**, 957 (1998).
[19] I.-H. Lee, V. Rao, R.M. Martin, and J.P. Leburton, Phys. Rev. B **57**, 9035 (1998).
[20] M. Rontani, F. Rossi, F. Manghi, and E. Molinari, Phys. Rev. B **59**, 10 165 (1999).
[21] C. Yannouleas and U. Landman, Phys. Rev. Lett. **82**, 5325 (1999).
[22] D. Babić, R. Tsu, and R.F. Greene, Phys. Rev. B **45**, 14 150 (1992).
[23] L. Bányai, P. Gilliot, Y.Z. Hu, and S.W. Koch, Phys. Rev. B **45**, 14 136 (1992).
[24] T. Takagahara, Phys. Rev. B **47**, 4569 (1993).
[25] M. Lannoo, C. Delerue, and G. Allan, Phys. Rev. Lett. **74**, 3415 (1995); G. Allan, C. Delerue, M. Lannoo, and E. Martin, Phys. Rev. B **52**, 11 982 (1995).
[26] J.M. Ferreyra and C.R. Proetto, Phys. Rev. B **57**, 9061 (1998).
[27] G. Goldoni, F. Rossi, and E. Molinari, Phys. Rev. Lett. **80**, 4995 (1998).
[28] A. Franceschetti and A. Zunger, Phys. Rev. Lett. **78**, 915 (1997).
[29] A. Franceschetti, H. Fu, L.W. Wang, and A. Zunger, Phys. Rev. B **60**, 1819 (1999).
[30] L.W. Wang and A. Zunger, Phys. Rev. B **51**, 17 398 (1995).
[31] A. Williamson and A. Zunger, Phys. Rev. B **61**, 1978 (2000).
[32] H. Fu and A. Zunger, Phys. Rev. B **55**, 1642 (1997).
[33] L.W. Wang and A. Zunger, J. Chem. Phys. **100**, 2394 (1994); J. Phys. Chem. **98**, 2158 (1994).
[34] L.W. Wang and A. Zunger, J. Chem. Phys. **100**, 2394 (1994); J. Phys. Chem. **98**, 2158 (1994).
[35] L.W. Wang and A. Zunger, in *Semiconductor Nanoclusters*, edited by P.V. Kamat and D. Meisel (Elsevier, Amsterdam, 1996).
[36] R. Resta, Phys. Rev. B **16**, 2717 (1977).
[37] H. Haken, Nuovo Cimento **10**, 1230 (1956).
[38] In the EMA calculation of $\Sigma_i^{\rm pol}$ we have neglected the small contribution originating from the $l>0$ terms in the sum of Eq. (30).
[39] C. Delerue, M. Lannoo, and G. Allan, Phys. Rev. Lett. **84**, 2457 (2000).
[40] F. Reboredo, A. Franceschetti, and A. Zunger, Phys. Rev. B **61**, 13 073 (2000).
[41] F. Reboredo, A. Franceschetti, and A. Zunger, Appl. Phys. Lett. **75**, 2972 (1999).
[42] S. Öğüt, J.R. Chelikowsky, and S.G. Louie, Phys. Rev. Lett. **79**, 1770 (1997).
[43] R.W. Godby and I.D. White, Phys. Rev. Lett. **80**, 3161 (1998).
[44] A. Franceschetti, L.W. Wang, and A. Zunger, Phys. Rev. Lett. **83**, 1269 (1999).